Report of Investigation 2026-2

Landslide mapping and susceptibility modeling on Wrangell Island, Alaska

Jillian A. Nicolazzo

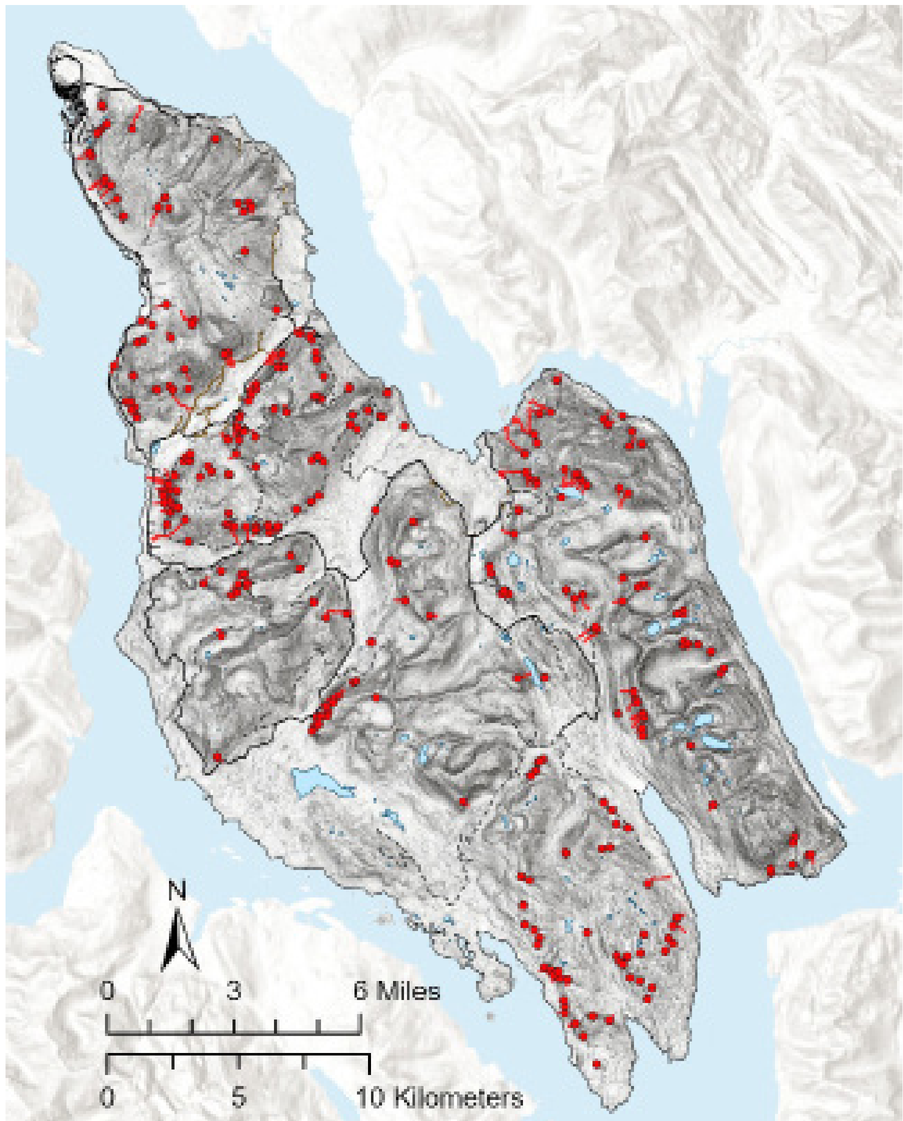

State of Alaska
Department of Natural Resources
Division of Geological & Geophysical Surveys

Landslide mapping and susceptibility modeling on Wrangell Island, Alaska

Jillian A. Nicolazzo

Report of Investigation 2026-2

State of Alaska
Department of Natural Resources
Division of Geological & Geophysical Surveys

State of Alaska
Mike Dunleavy, Governor

Department of Natural Resources
John Crowther, Commissioner

Division of Geological & Geophysical Surveys
Erin A. Campbell, State Geologist & Director

Publications produced by the Division of Geological & Geophysical Surveys (DGGS) are available for free download from the DGGS website (dggs.alaska.gov). Publications on hard-copy or digital media can be examined or purchased in the Fairbanks office:

Alaska Division of Geological & Geophysical Surveys
3354 College Rd., Fairbanks, Alaska 99709-3707
Phone: (907) 451-5010 Fax (907) 451-5050
dggspubs@alaska.gov

DGGS publications are also available at:
Alaska State Library
Historical Collections & Talking Book Center
395 Whittier Street
Juneau, Alaska 99801

Alaska Resource Library and Information Services (ARLIS)
Library Building, Suite 111
3211 Providence Drive
Anchorage, AK 99508

Suggested citation: Nicolazzo, J.A. 2026, Landslide mapping and susceptibility modeling on Wrangell: Alaska Division of Geological & Geophysical Surveys Report of Investigation 2026-2, 21 p., 3 sheets. https://doi.org/10.14509/32057

Contents

Figures

Tables

Landslide Mapping and Susceptibility Modeling on Wrangell Island, Alaska

Jillian A. Nicolazzo[1]

Abstract

The fatal 2023 Zimovia Highway landslide reinforced the safety and financial risks that slope failures pose to people and infrastructure on Wrangell Island, Alaska. To improve the City and Borough of Wrangell's resilience to landslide hazards, the Alaska Division of Geological & Geophysical Surveys (DGGS) expanded an existing landslide inventory and modeled shallow landslide susceptibility and potential debris flow inundation.

The landslide inventory integrates previously mapped landslides in the Tongass National Forest with newly mapped slope failures. More than 90 percent of the inventoried features are classified as debris flows. DGGS evaluated shallow landslide susceptibility using frequency ratio analysis of inventoried landslides and terrain factors that influence landslide occurrence. The highest susceptibility is associated with slopes steeper than 31° that are southwest- to west-facing, in close proximity to drainages, and comprised of colluvial soils. Model performance was strong, with an area under the receiver-operating characteristic curve of 0.88. DGGS modeled the potential for channelized debris flows to initiate and flow downslope and the inundation extents. Inundation was modeled for relatively common events that might occur every few years to decades, and rare events that might occur once in 1,000 years. Collectively, the results of these analyses provide a regional assessment of landslide hazards on Wrangell Island and can help guide future land-use planning and development, and other scientific investigations.

Introduction

Two large landslides occurred on November 20, 2023, on Wrangell Island, Alaska. The first reported landslide crossed the Zimovia Highway near milepost 11.2. It destroyed homes, caused six fatalities, downed utility lines, and cut off access to the town for residents south of the landslide. The second landslide occurred nearby on Middle Ridge Road. It crossed the switch-back road in three places and temporarily stranded one person between the upper two crossings. Through lidar data comparison, Nicolazzo and others (2024) identified two additional, smaller landslides in the same area that they attributed to the same timeframe.

To support the City and Borough of Wrangell (CBW) in increasing landslide hazard resiliency, the Alaska Division of Geological & Geophysical Surveys (DGGS) received funding from the Federal Emergency Management Agency Cooperating Technical Partners Program to map landslide occurrences, and model shallow landslide susceptibility and channelized debris flow inundation for Wrangell Island. The CBW voted in support of this project on February 13, 2024.

This project includes all of Wrangell Island, an area of approximately 570 sq km (220 sq mi) (fig. 1). Wrangell Island is located about 250 km (155 miles) southeast of Juneau, and the city of Wrangell is at the northwest point of the island. The island occupies portions of the Bradfield Canal A-6 and B-6, and Petersburg A-1, B-1, and B-2 quadrangles.

This study is based on existing datasets and did not include field mapping or ground

[1]Alaska Division of Geological & Geophysical Surveys, 3354 College Rd., Fairbanks, Alaska 99709-3707.

verification. This report describes the datasets and methods used in this study and discusses the mapping and modeling results. Three 1:25,000 scale map sheets accompany this report:

- Map Sheet 1 Landslide Inventory
- Map Sheet 2 Shallow Landslide Susceptibility
- Map Sheet 3 Debris Flow Susceptibility and Inundation Modeling

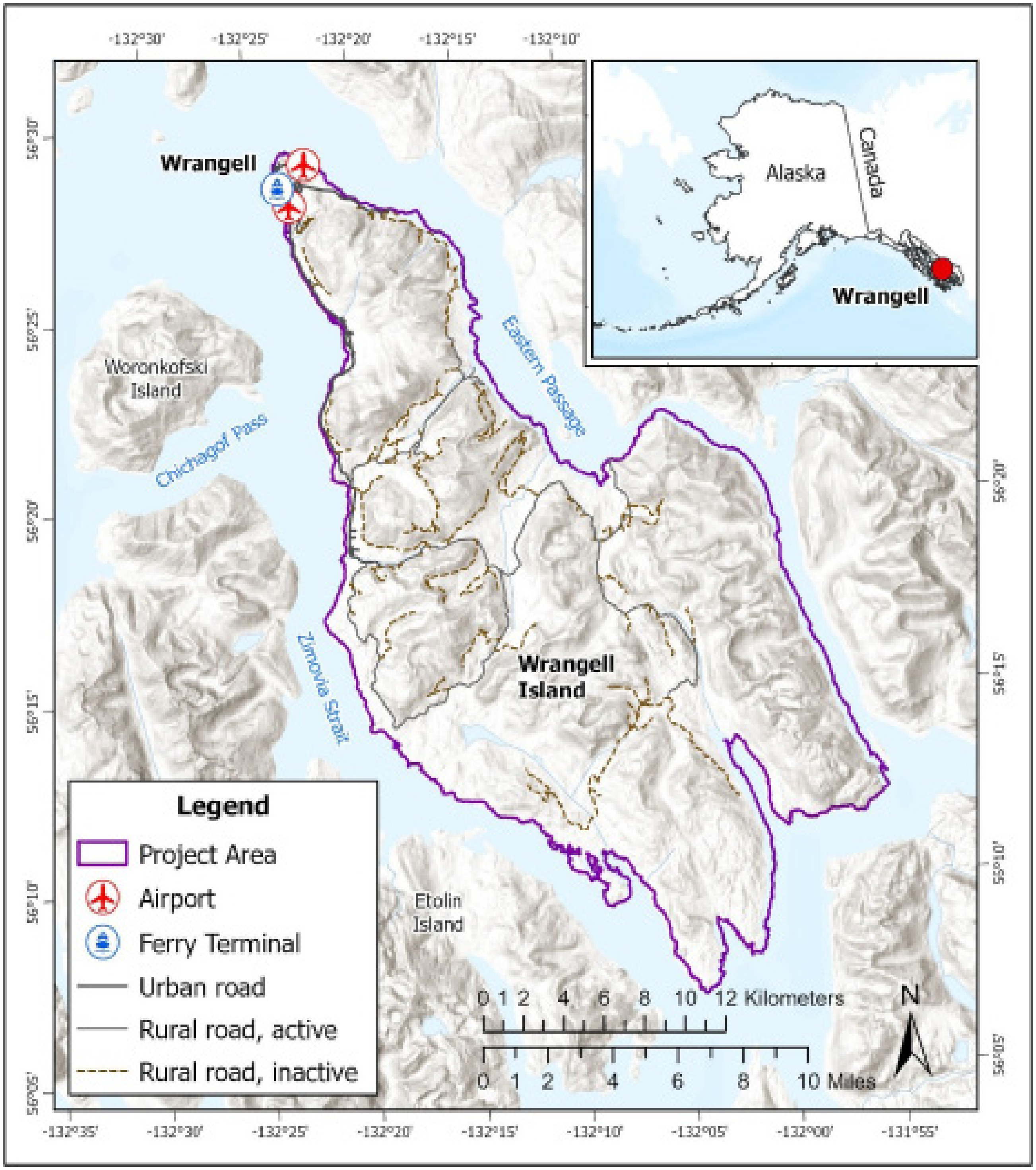

Figure 1. Figure showing this project's study area and major infrastructure displayed over Esri's World Terrain basemap.

Existing Data

Two 1:63,360-scale geologic maps of the Petersburg B-1 and B-2 quadrangles (Brew, 1997a; Brew, 1997b) were incorporated into a 1:150,000-scale map of the region by Karl and others (1999). These maps focused on bedrock geology and did not differentiate the surficial soils. Lemke (1974) produced a 1:7,200-scale map of surficial soils of the area immediately around the city of Wrangell. We obtained additional surficial soils information from the USDA STATGO2 soils database (U.S. Department of Agriculture, 2017), and wetlands data from the U.S. Fish & Wildlife Service (U.S. Fish & Wildlife Service, 2025).

Most of Wrangell Island lies within the Tongass National Forest (TNF), where the U.S. Forest Service maintains a database of mapped landslides and estimated landslide initiation locations that have occurred within the TNF boundary (U.S. Forest Service, 2024a; U.S. Forest Service, 2024b). The U.S. Forest Service created the inventory by digitizing landslides visible in orthoimagery. The databases were first published in 2019 and are continually updated.

DGGS previously collected two light detection and ranging (lidar) datasets on Wrangell Island. The July 2023 dataset includes all of Wrangell Island (Zechmann and others, 2023). The November 2023 dataset (Zechmann and others, 2024) was collected in response to the November landslides and includes priority areas. DGGS published a report comparing these two lidar datasets (Nicolazzo and others, 2024).

Methods

Landslide Inventory Geodatabase and Map

In this section, we use the term “landslide” generically to refer to all types of slope failures identified in the area, including landslides, debris flows, and rockfall. We followed the landslide inventory mapping protocols described by Burns and Madin (2009) and Slaughter and others (2017) to identify landslide deposits, flanks and scarps. We used the same database feature layers, attributes, and data dictionary as Nicolazzo and Larsen (2025a).

Using ArcGIS Pro, we created four feature classes for the inventory: deposit polygons, flank polygons, scarp polylines, and landslide initiation points; however, not all slope instabilities have all these features. The “ideal” translational or rotational landslide includes a head scarp, possible internal scarps, flanks, and a deposit, but we rarely identified all of these features. Additionally, debris flows that are confined to drainage channels generally lack a well-defined source area and do not originate at a scarp, so these deposit polygons do not have associated scarps or flanks. Rockfall deposits might have an associated scarp polyline but no flank polygon. Erosional deposits such as colluvium and talus were not classified as landslides, but we mapped scarp polylines for some because their presence indicates the bedrock is unstable in these areas and falling rock could pose a hazard. Initiation points are approximately located or inferred based on the presence of a visible scarp, or the uppermost extent of visible scour.

We incorporated the TNF landslide inventory (U.S. Forest Service, 2024a; U.S. Forest Service, 2024b), excluding snow avalanches, into our database and used it as calibration for identifying other slope failures on Wrangell Island. We also included slope failures identified by others (Nicolazzo and others, 2024, Alaska Department of Transportation & Public Facilities, 2022). Through interpretation of hillshade and slope rasters derived from lidar-based digital terrain models (DTMs), we then identified additional slope failures in the study area. Review of aerial imagery from publicly available sources, including DGGS’ 50-centimeter Maxar, Esri Wayback, and Google Earth supplemented the DTMs. We identified additional slope failures throughout the project period. Each of the mapped landslides may represent a single occurrence, or multiple events. The resultant inventory map is shown on map sheet 1. A data dictionary accompanies the database.

Shallow Landslide Susceptibility Modeling

Shallow landslides are downslope movements of soil or rock that occur within the uppermost layers, typically within surficial soils. Shallow landslides are generally defined as having a failure plane less than 3 to 4.5 m (10 to 15 ft) deep. This modeling does not include deep-seated bedrock failures or ground failures triggered by seismic shaking, such as liquefaction or lateral spread, which require site-specific information and are outside the scope of this project. Additionally, shallow landslide susceptibility does not include channelized debris flow inundation, which is discussed in the next section.

Initially, we followed the methodology of Burns and others (2012), which combines mapped shallow landslides with calculated factors of safety based on soil strength and slope angles to produce a map of landslide susceptibility zones. DGGS successfully used this method in Sitka (Hubbard and others, 2025), Homer (Salisbury, 2024), and Haines (Nicolazzo and Larsen, 2025b); however, for this project, this resulting susceptibility distribution did not match the landslide inventory. We interpreted this mismatch as primarily resulting from limited soil engineering property data. The method may also be less applicable to the types of slope failure that dominate Wrangell Island, where many failures initiate outside of flow channels and then transition into debris flows.

As an alternative, we adopted a data-driven statistical approach to model shallow landslide susceptibility. The inventory of mapped landslides, described above, provided the dataset for frequency ratio (FR) analysis. We used FR analysis to quantify statistical relationships between landslide occurrence and terrain attributes. We evaluated model performance using area under the curve (AUC) analysis. AUC values quantify how well the susceptibility model distinguishes locations with and without mapped landslides. The resulting map categorizes landslide susceptibility from very low/none to very high (map sheet 2).

Frequency Ratio

Frequency ratio (FR) is a data-driven statistical method that quantifies how strongly a landslide conditioning factor is associated with known landslides. The method requires a robust landslide inventory and a set of data layers that may influence landslide occurrence, for example slope angle, aspect, and geology. Each data layer is divided into classes, or "bins", and the percent of landslides in each bin is compared to how much of the study area that bin occupies (eq. 1). Bin sizes for each conditioning factor were selected and refined based on data distribution to capture meaningful variation while maintaining adequate sample size within each class.

This ratio indicates whether landslides occur more or less frequently in a given bin than would be expected based on its area. Values less than 1.0 indicate a lower association with mapped landslides, while values greater than 1.0 indicate a stronger association. FR values are then combined to calculate the Final Frequency Ratio (FFR, eq. 2) to create the final landslide susceptibility map (Lee and Talib, 2005; Strauch and others, 2019). Higher values indicate areas where the combination of conditioning factors has a stronger statistical association with mapped landslides.

$$\mathrm{FR} = \frac{N_{pi}/N}{A_{pi}/A} \qquad (1)$$

Where N_{pi} is the number of landslides in each bin (i) for each contributing factor (p) and N is the total number of landslides investigated. A_{pi} is the area of each bin (i) for each contributing factor (p) and A is the total study area.

$$FFR = \sum FR \qquad (2)$$

The results of the FR calculations are provided in table 1. For example, two inventoried landslides occurred within the slope angle bin of 0 to 11°, and that slope angle bin includes 179.05 sq km (69 sq mi) of area. We examined 275 landslides extracted from the landslide inventory database distributed across the 568.82 sq km (219 sq mi) study area; therefore, the FR for the 0 to

11° slope angle bin is:

$$FR_{Slope\ Bin\ 0-11^{\circ}} = \frac{2/275}{179.05/568.82} = \frac{0.0073}{0.3148} = 0.02$$

We initially evaluated slope angle, slope aspect, slope curvature, distance to drainage, distance to roads, geology, and topographic wetness index as potential conditioning factors. After calculating FR values and evaluating model performance using AUC, we selected four factors, slope angle, slope aspect, distance to drainage, and geology, to produce the final susceptibility map (map sheet 2). Results for all evaluated factors are presented here.

We evaluated these factors for 275 inventoried landslide initiation points. We buffered the initiation points by 3m (~10 ft) to create small polygons that could be used with the Zonal Statistics geoprocessing tool to extract the average slope angle, aspect, and curvature values for each polygon from the July 2023 DTM (Zechmann and others, 2023). These values were assigned to the initiation points. We used the Near tool to obtain distances from each initiation point to drainages and roads. We then resampled the DTM (Zechmann and others, 2023) to 3 m (~10 ft) resolution for processing efficiency, which is also the resolution of the final susceptibility map. Because the lidar data were collected after most of the mapped landslides occurred, the DTM represents post-landslide topography, which means landslide initiation points may appear steepened or planar due to the presence of landslide scarps.

Slope Angle

Slope angle is one of the most important factors influencing landslide initiation (Highland and Bobrowski, 2008; Burns and others, 2022). The mean slope angle of the 275 landslide initiation sites is 41° (standard deviation 7°). Very few initiation sites had mean slope angles less than 16° or greater than about 60°, and the number of mapped initiation sites increased notably at 32° (fig. 2). Slopes steeper than about 55° are generally considered too steep to retain sufficient soil or colluvium for shallow landslides to occur (Burns and others, 2022). Instead, failures at these steep angles may occur as rockfall or rock topple.

Slope Aspect

Many of the 275 landslides occurred on south- to west-facing slopes, which may reflect the influence of bedrock structure, increased exposure to marine weathering and prevailing weather, or other environmental controls. Because we do not have data to directly evaluate these processes, we used aspect as a proxy for other potential

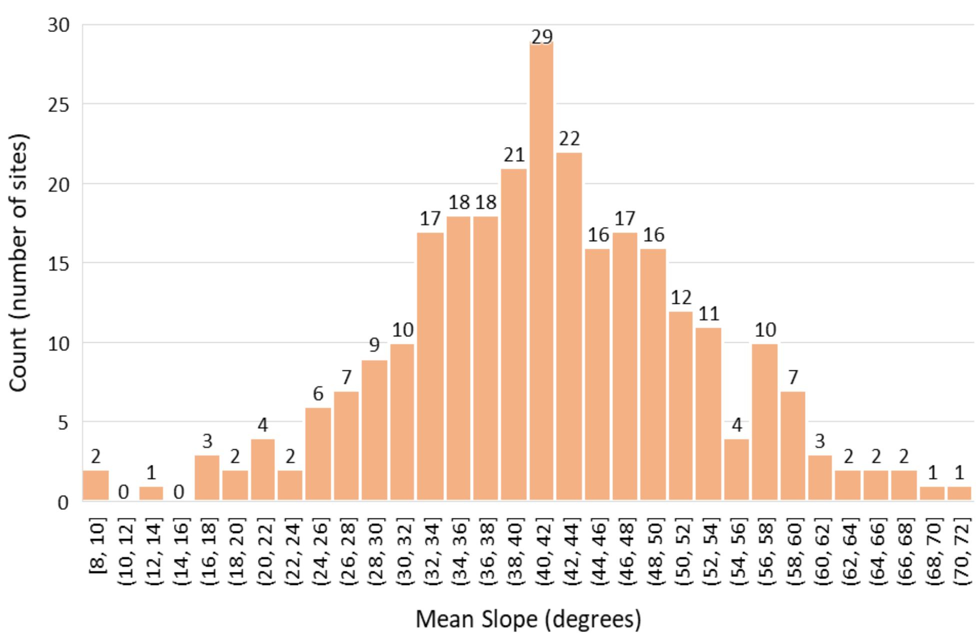

Figure 2. Histogram of slope angle (in degrees) at landslide initiation sites.

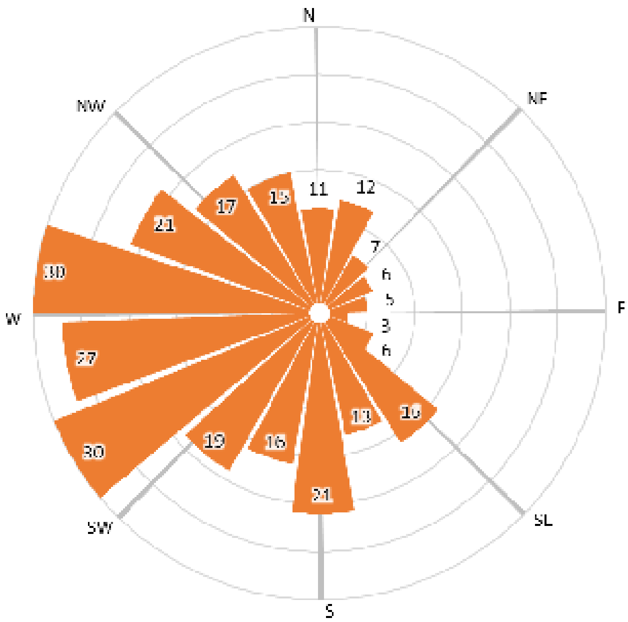

Figure 3. Rose diagram showing landslide occurrence categorized by slope aspect (in degrees).

contributing factors.

The mean aspect of the landslide initiation sites is 217° (standard deviation 18°) (fig. 3), which corresponds to a southwest-facing slope. The rose diagram shows 45 percent of inventoried landslides occurred on southwest- and west-facing slopes, with an additional 15 percent occurring on northwest-facing slopes. The higher proportion of landslides on southwest- to west-facing slopes resulted in higher FR values for those aspect classes.

Curvature

Curvature provides information about the shape of the slope, indicating where the topography is convergent or divergent (Burns and others, 2022). Negative values correspond to convergent areas, where water and soil might accumulate. Positive values correspond to divergent areas, where water and soil may be dispersed. A curvature value of zero indicates planar topography that is neither convergent nor divergent. According to Esri's documentation, curvature values for hilly terrain with moderate relief can range from -0.5 to 0.5, whereas steep, rugged terrain with extreme relief can range from -4 to 4 with greater values possible (Esri, n.d.).

The mean planform curvature of the landslide initiation sites is -0.05 (standard deviation 0.12), indicating near planar topography (fig. 4). Profile curvature (not shown here) also indicates planar topography. This suggests that most mapped landslide initiation sites are not strongly associated with either convergent or divergent topography; therefore, curvature was not included in the final susceptibility model.

Distance to Drainages

In addition to slope angle, the presence of water is a major factor influencing landslide initiation. During lidar data interpretation, we observed that many of the inventoried landslides on Wrangell Island are near incised drainage channels. Because soil moisture data were unavailable, and rainfall data are limited to the northern end of the island, we used distance to drainages as a proxy for hydrologic influence.

We used the drainage network generated as part of the Channelized Debris Flow Inundation Modeling described in the next section to measure the distance between each landslide initiation point and the nearest drainage. The median distance is 44 m (144 ft), although a small number of distant outliers increase the mean distance to 75 m (246 ft). Forty percent of the landslides occur within 30 m (98 ft) of a drainage (fig. 5). Restricting the analysis to initiation sites within 150 m (~500 ft) of a drainage channel reveals that 15 percent occur within 5 m (16 ft) and the association quickly decreases at farther distances (fig. 6). We used this distribution to select the bins used in analysis.

Distance to Roads

Distance to roads has been evaluated as a conditioning factor in previous landslide susceptibility studies (Es-smairi, 2023). Although numerous roads are visible in aerial imagery and the lidar DTM for Wrangell Island, many are not included in published GIS datasets, and those that are included may not always align accurately with the DTM; therefore, we digitized all visible roads into a new feature layer for use in this analysis. This feature layer includes paved, active roads, unpaved rural roads, and decommissioned rural

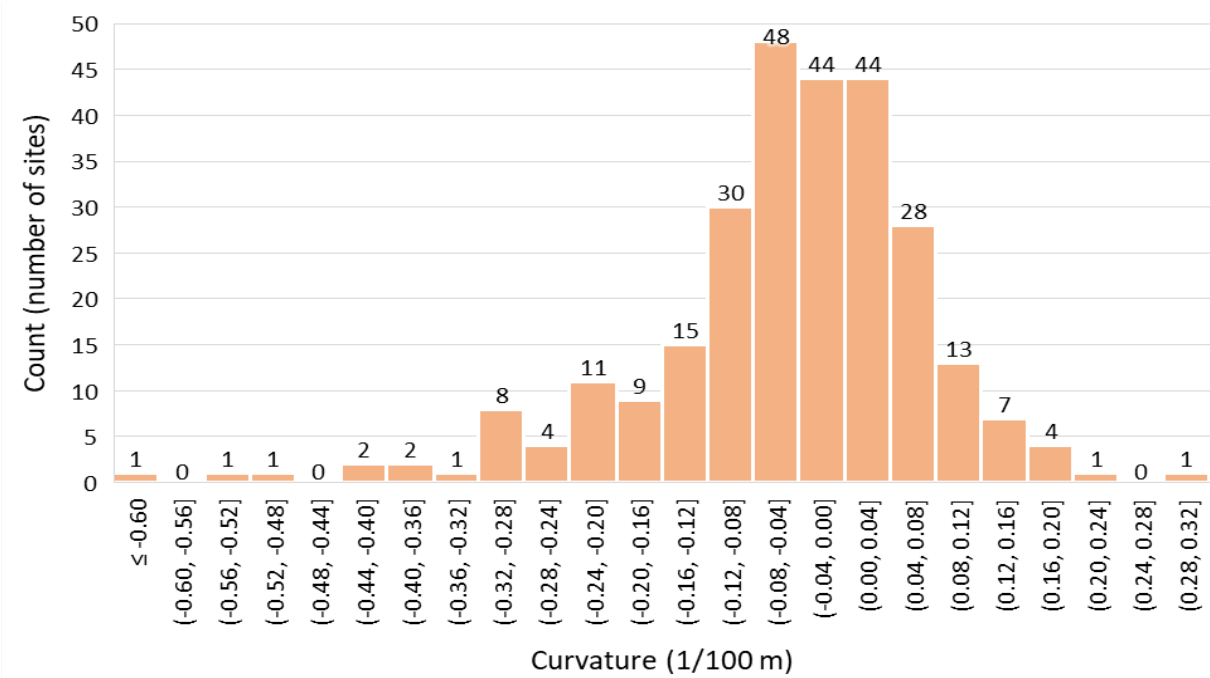

Figure 4. Histogram of curvature at landslide initiation sites.

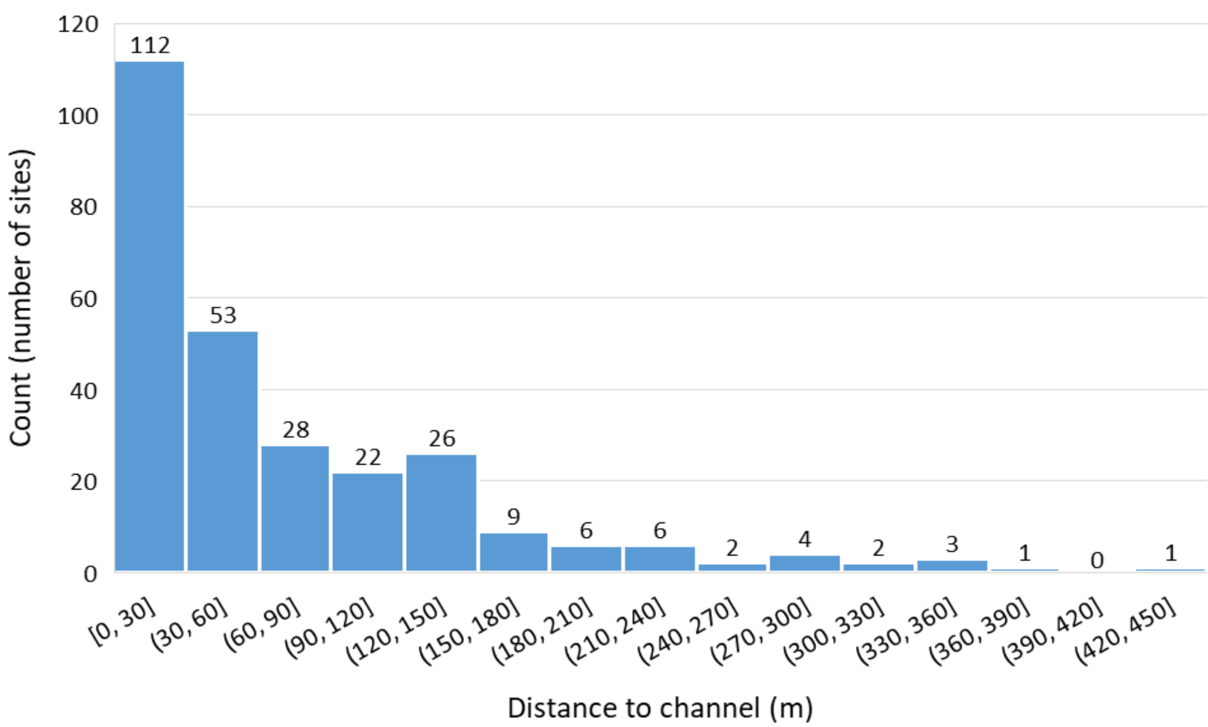

Figure 5. Histogram of distance between landslide initiation sites and drainages.

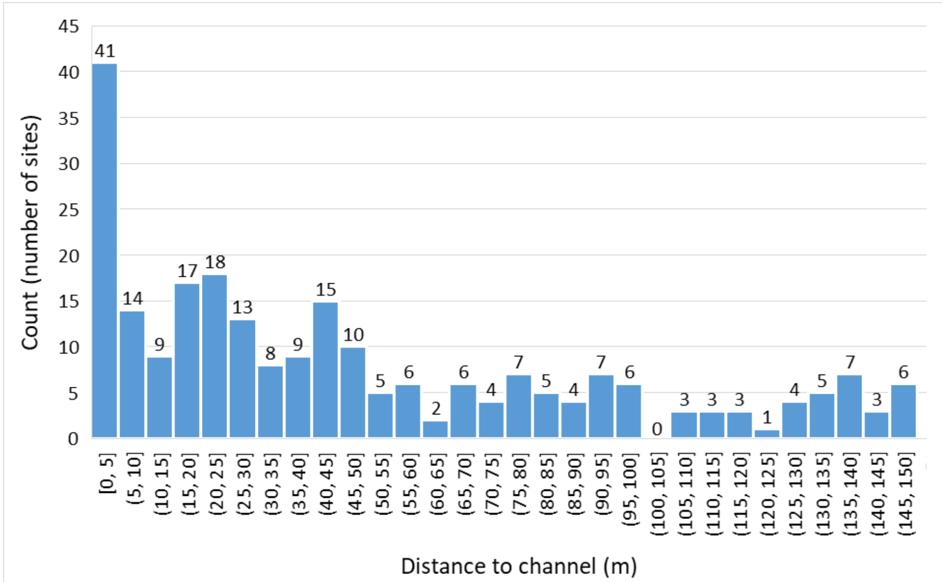

Figure 6. Histogram of distance between landslide initiation sites and drainages, limited to 150m.

roads. Because the status of some rural roads is unknown, we treated them all equally.

Only 20 landslide initiation points are within 30 m (98 ft) of a road, indicating a weak association between landslide initiation and road proximity. Consequently, distance to roads was not included in the final susceptibility model.

Geology

Geology is an important conditioning factor for landslide initiation. Although a detailed surficial geologic map exists for the area surrounding the City of Wrangell (Lemke, 1974), geologic mapping for much of Wrangell Island is generalized and does not include surficial soils (Brew 1997a; Brew, 1997b; Karl and others, 1999). Portions of the island have not been mapped. We combined these geologic maps, soil data from the U.S. Department of Agriculture (2017), and the U.S. Fish & Wildlife Service (2025) to develop a surficial soils map for use in this study. Where data overlapped or conflicted, we refined soil unit contacts or digitized additional boundaries based on aerial imagery and the lidar DTM.

Landslide initiation points occur within four mapped soil and bedrock units on Wrangell Island. Fifty percent initiated in bedrock (approximately equal numbers in hornfels, and tonalite/tonalite porphyry), 41 percent in colluvium, 8 percent in colluvium-alluvium, and 1 percent in glacial outwash. No inventoried landslides initiated in areas mapped as wetlands by the U.S. Fish & Wildlife Service (2025). These percentages describe the distribution of inventoried landslides among geologic units. The corresponding FR values account for the relative area of each geologic unit (table 1).

Topographic Wetness Index

Topographic wetness index (TWI) estimates how water accumulates and how likely an area is to remain saturated. Some landslide studies use TWI as a proxy for soil moisture content (Strauch and others, 2019). We calculated TWI in GIS using the lidar DTM and the Flow Direction, Flow Accumulation, and Slope geoprocessing tools, and eq. 3 (Beven and Kirkby, 1979).

$$TWI = \ln\left(\frac{A_s}{\tan\beta}\right) \quad \textbf{(3)}$$

Where A_s is the upslope contributing area per unit contour length (i.e. the Flow Accumulation raster), and β is the slope angle in radians. High TWI values correspond to flat or gently sloping, convergent topography and indicate areas where water is more likely to accumulate, potentially resulting in higher soil moisture. Conversely, low TWI values are characteristic of steep terrain and indicate divergent flow paths, resulting in lower soil moisture contents.

The mean TWI of landslide initiation sites is 2.9 (standard deviation 2.4) (fig. 7), which is consistent with relatively dry ridges and well-drained slopes. Because TWI incorporates slope angle and is indirectly influenced by terrain convergence through flow accumulation, TWI may provide information that is largely redundant when these factors are considered separately. We showed previously that the study area has steep slopes and planar topography, so TWI was not included in the final susceptibly model.

Frequency Ratio Value

The final susceptibility model includes four conditioning factors: slope angle, slope aspect, distance to drainage, and geology. Using equation 1, we calculated an FR value for each bin of every conditioning factor; the results are summarized in table 1. An FR value of 1.0 indicates an average frequency of landslide occurrence for that factor and bin. FR values less than 1.0 indicate a weaker association with mapped landslides, and values greater than 1.0 indicate a stronger association.

We first classified slope angle and aspect rasters by bin values (table 1) and then reclassified each bin by its corresponding FR value (table 1). We buffered drainage polylines to create polygons representing each distance bin and converted the resulting polygons to rasters classified by their corresponding FR values. We also converted the geology polygons to rasters and classified them by their corresponding FR values. We then mosaicked the rasters and used raster algebra to sum the FR values (eq. 2) to produce the final landslide susceptibility raster shown on map sheet 2.

The average summed FR value for landslide initiation sites is 9.90 (standard deviation 5.18). Because the final susceptibility is the sum of four FR values, a summed FR value of 4.0 represents the theoretical expectation if each conditioning factor has an average FR of 1.0. The histogram shows that few inventoried landslides have summed FR values below 4.0 and that most occur at substantially higher values (fig. 8). This indicates that landslides on Wrangell Island commonly occur where multiple conditioning factors are simultaneously associated with landslide initiation. We used this

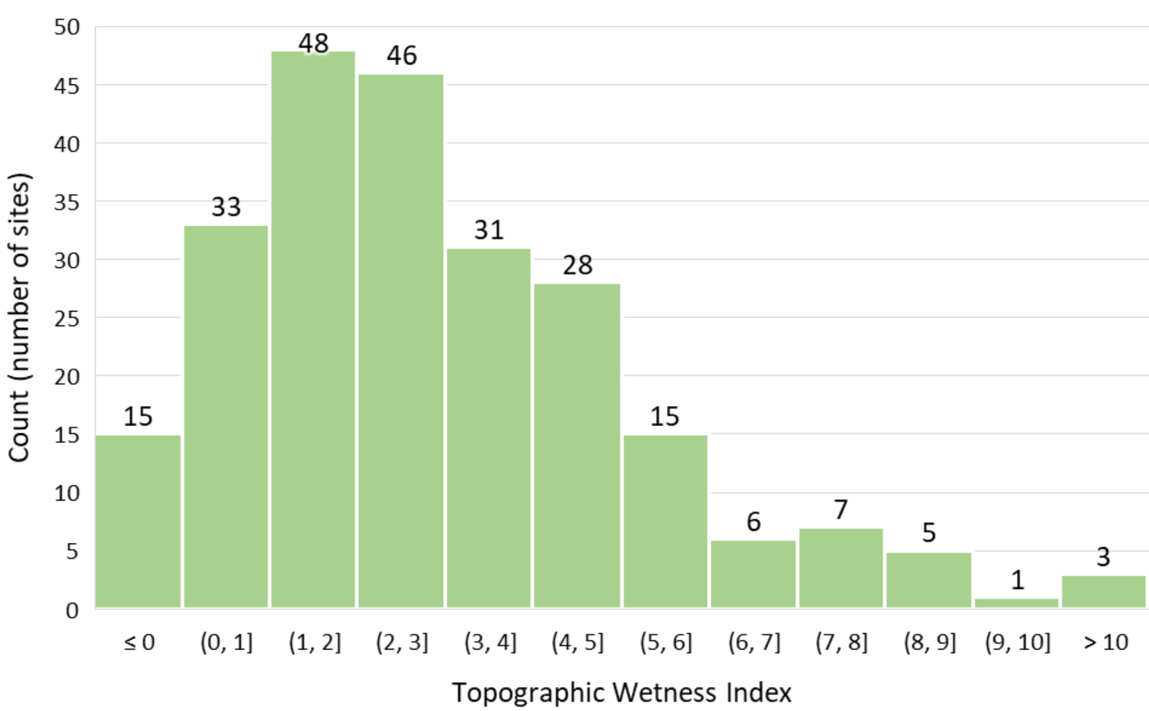

Figure 7. Histogram of topographic wetness index at landslide initiation sites.

Table 1. Frequency ratio of landslide conditioning factors

Factor	Bin	Landslide occurrence (count) (n=270)	Landslide occurrence (percent)	Area (km^2) (total= 568.82)	Area (percent)	Frequency Ratio
Slope Angle (deg)	<=11	2	0.73	179.05	31.48	0.02
	11 <= 15	1	0.36	66.39	11.67	0.03
	15 <= 19	4	1.45	60.27	10.59	0.14
	19 <= 23	5	1.82	55.76	9.80	0.19
	23 <= 27	12	4.36	51.19	9.00	0.48
	27 <= 31	18	6.55	44.89	7.89	0.83
	31 <= 35	27	9.82	37.42	6.58	1.49
	35 <= 39	39	14.18	29.07	5.11	2.77
	39 <= 43	46	16.73	19.50	3.43	4.88
	43 <= 47	39	14.18	11.19	1.97	7.21
	47 <= 51	32	11.64	6.35	1.12	10.42
	51 <= 55	21	7.64	3.61	0.63	12.03
	55 <= 59	16	5.82	2.01	0.35	16.46
	59 <= 63	6	2.18	1.12	0.20	11.10
	63 <= 67	4	1.45	0.58	0.10	14.22
	67 <= 71	3	1.09	0.27	0.05	22.88
	71+	0	0.00	0.15	0.03	0.00
Aspect (deg)	N	28	10.18	58.49	10.28	0.99
	NE	15	5.45	76.72	13.49	0.40
	E	9	3.27	87.88	15.45	0.21
	SE	26	9.45	74.04	13.02	0.73
	S	33	12.00	63.45	11.16	1.08
	SW	58	21.09	75.59	13.29	1.59
	W	65	23.64	71.56	12.58	1.88
	NW	41	14.91	61.10	10.74	1.39
Distance to drainage (m)	<= 30	112	40.73	132.35	23.27	1.75
	30 <= 60	53	19.27	91.70	16.12	1.20
	60 <= 90	28	10.18	67.65	11.89	0.86
	90 <= 120	22	8.00	52.19	9.18	0.87
	120 <= 150	26	9.45	41.31	7.26	1.30
	150 <= 180	9	3.27	32.47	5.71	0.57
	180 <= 210	6	2.18	25.36	4.46	0.49
	210 <= 240	6	2.18	19.98	3.51	0.62
	240 <= 270	2	0.73	15.65	2.75	0.26
	270 <= 300	4	1.45	12.26	2.15	0.68
	300+	7	2.55	77.42	13.61	0.19

Factor	Bin	Landslide occurrence (count)	Landslide occurrence (percent)	Area (m^2)	Area (percent)	Frequency Ratio
Geology	Bedrock	139	50.5	249.41	43.8	1.15
	Colluvium	112	40.7	87.63	15.4	2.64
	Colluvium-alluvium	22	8.0	99.58	17.5	0.46
	Glacial outwash	2	0.7	25.50	4.5	0.16
	All others	0	0.0	106.71	18.8	0.00

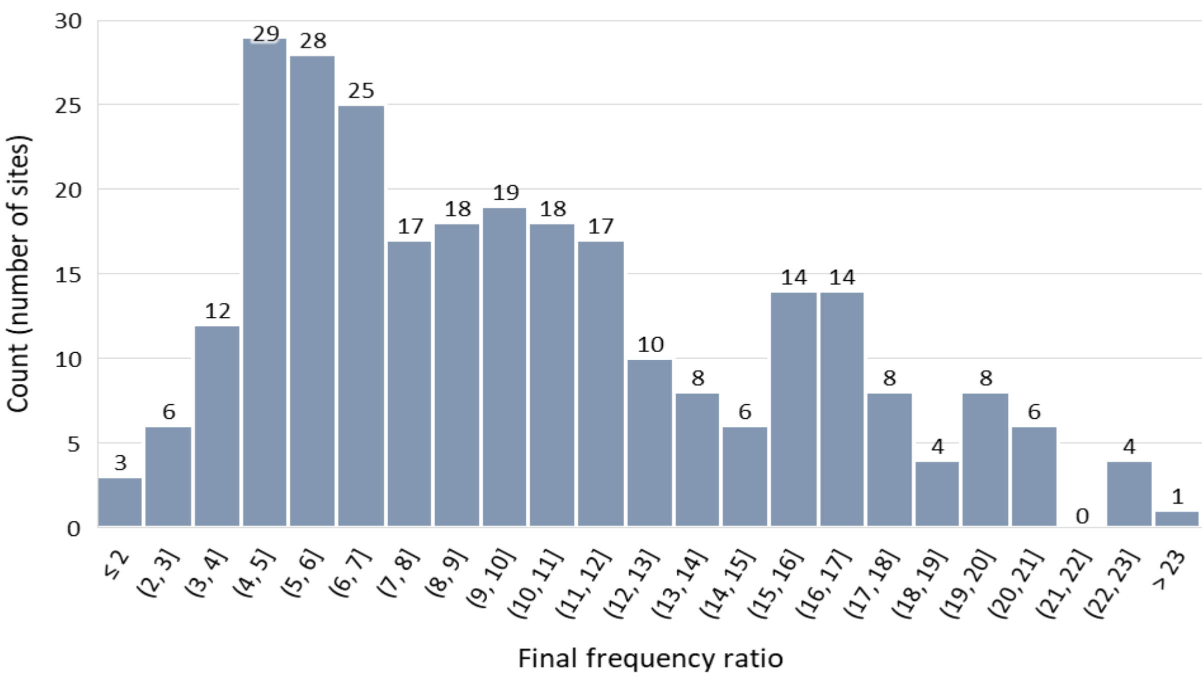

Figure 8. Histogram of the final frequency ratio values at landslide initiation sites.

observed distribution of summed FR values, along with professional judgment, to define the final susceptibility class boundaries.

We selected a summed FR value of 3.2 as the lower boundary of the low susceptibility classification. This value corresponds to an average FR value of 0.8 for each of the four conditioning factors and is lower than the theoretical expected summed FR value of 4.0. Four percent of inventoried landslides have summed FR values below this threshold. We defined the lower boundary of the moderate susceptibility classification as one standard deviation below the mean summed FR value (4.72). We used the mean summed FR value (9.90) as the lower boundary of the high susceptibility classification.

The highest summed FR values correspond to slopes steeper than about 50° that are west-facing and are within 30 m (~100 ft) of a drainage. These slopes are generally composed of bedrock because they are too steep to retain significant colluvium. The corresponding individual FR values are 10.42 for slope angle, 1.88 for slope aspect, 1.75 for distance to drainage, and 2.64 for bedrock (table 1), yielding a summed FR value of 15.16. This value closely matches the mean plus one standard deviation, 15.08, which we selected as the upper boundary of the high susceptibility classification.

We classified summed FR values greater than 15.08 as very high susceptibility. This class is dominated by very steep bedrock slopes, where failures are more likely to occur as rockfall or rock topple and may accumulate downslope as talus deposits. Although this classification covers only a small percentage of the study area, it contains 21 percent of the inventoried landslide initiation sites. The susceptibility classification thresholds are summarized in table 2.

Table 2. Landslide susceptibility classification thresholds

Susceptibility Classification	Summed FR
Very Low to None	<=3.2
Low	3.2 <= 4.72
Moderate	4.72 <= 9.90
High	9.90 <= 15.08
Very high	> 15.08

Area Under the Curve

We evaluated the performance of the FR landslide susceptibility model using receiver-operating characteristic (ROC) analysis. The ROC curve illustrates how well the model distinguishes landslide areas from non-landslide areas. The area under the curve (AUC) is a value between 0.0 and 1.0 that summarizes the performance of the ROC curve. An AUC value of 0.5 corresponds to a straight line from (0,0) to (1,1) and indicates that the model performs no better than random chance. A curve and value closer to 1 indicate the model is correctly predicting landslides (Fawcett, 2006, Lee and Talib, 2005).

To construct the ROC curve and calculate AUC, we used 275 landslides extracted from the landslide inventory and their associated summed FR value, described above. We then generated 275 random, non-landslide points to provide an equal number of positive and negative observations for model evaluation. To generate the random points, we buffered the landslide polygons by 10 m (32.8 ft) and masked these areas to ensure the non-landslide points were not within or immediately adjacent to a known landslide. We distributed the random points at least 30 m (~100 ft) apart to minimize clustering. Finally, we extracted values from the summed FR raster for the non-landslide points.

We calculated the true positive rate (TPR) and false positive rate (FPR) for the landslide and non-landslide points and plotted these values to create the ROC curve (fig. 9). Four possible outcomes contribute to the ROC curve. A known landslide point with a high summed FR value is a true positive (TP), indicating that the model correctly identified a landslide. A non-landslide point with a high summed FR value is a false positive (FP), indicating that the model incorrectly predicted a landslide. A non-landslide point with a low summed FR value is a true negative (TN), indicating that the model correctly identified a stable location. A known landslide point with a low summed FR value is a false negative (FN), indicating that the model failed to identify a landslide. The TPR is calculated by dividing TP by the total number of positives, and the FPR is calculated by dividing FP by the total number of negatives (Fawcett, 2006).

We calculated ROC in Excel following the steps explained by Bobbitt (2021). We first sorted

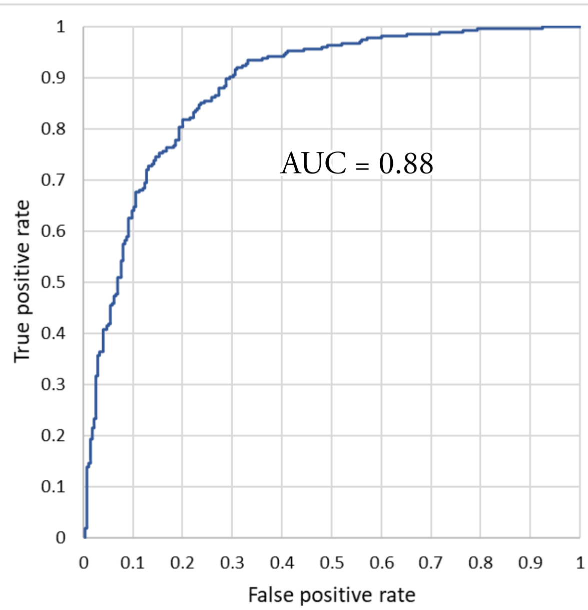

Figure 9. Reciever-operating characteristic (ROC) curve and area under the curve (AUC).

the landslide and non-landslide points together by their summed FR values in descending order and evaluated the classification at each unique FR threshold. At each threshold, we calculated the cumulative numbers of TP and FP, from which the TPR and FPR were calculated. The ROC curve was constructed by plotting the TPR against the FPR for all thresholds. We used the trapezoidal rule to calculate the AUC (eq. 4). For the final susceptibility model, which includes slope angle, slope aspect, geology, and distance to drainage, the AUC is 0.88 indicating very good model performance.

$$AUC = \sum\left((FPR_{i+1} - FPR_i) * \frac{TPR_i + TPR_{i+1}}{2}\right) \quad (4)$$

Channelized Debris Flow Inundation Modeling

Debris flows are a form of mass movement characterized by a slurry of water, soils, rocks, trees, and other debris quickly moving down slope under the influence of gravity. They are often associated with large rain events and are among the most destructive and expensive geohazards that occur in Alaska (Division of Homeland Security & Emergency Management, 2023). Channelized debris flows often initiate as a shallow landslide entering a channel, or erosion within or directly adjacent to a channel, that then flows down the channel eroding and entraining additional material as it flows until it reaches a flatter or less confined ground, where the flow then slows and material is deposited (Burns and others, 2022).

Laharz is a computer model developed for the U.S. Geological Survey (USGS) that simulates the behavior of volcanic mudflows, known as lahars, and was modified to include channelized debris flows (Schilling, 1998). Burns and others (2022) extended the Laharz model to include the ability for volumes to expand as they flow down the channel. Burns and others (2022) produced custom ArcGIS geoprocessing tools to simplify the process. The method models debris flow initiation potential, transport potential, and inundation (deposition) to produce a map that displays debris flow initiation and transport susceptibility as watersheds having high, moderate, or low susceptibility, and the inundation extent for each level of modelled event severity (map sheet 3).

Initiation

Nicolazzo and Larsen (2025b) evaluated whether the debris flow modeling parameters proposed by Burns and others (2022) are appropriate for southeast Alaska. Using the TNF landslide initiation point database (U.S. Forest Service, 2024b) and the Wrangell Island elevation data (Zechmann and others, 2023), they found that the average slope closely matches that reported by Burns and others (2022), but curvature values differ, suggesting that the curvature value should be adjusted for southeast Alaska.

The protocol developed by Burns and others (2022) identifies drainage channels using a curvature-based method. They used a concavity threshold of -2.0 but this value underrepresents drainage networks on Wrangell Island, which resulted in known debris flow channels being excluded from the analysis. We tested various combinations and determined that a concavity threshold of -1.2 better represented the observed drainage network on Wrangell Island. When multiple iterations were run, the minimum concavity size and contributing concave area inputs did not appear to change the output significantly, so we retained the values of 10 m^2 (107.6 ft^2) and 200 m^2 (2,152.8 ft^2), respectively, recommended by Burns and others (2022). We also used these values to model deposition, described in the Inundation/Deposition section of this report.

Using values suggested by Burns and others (2022), we assigned values of 1 to 4, corresponding to no, low, moderate, and high susceptibility, respectively, to a range of slope and curvature raster values. Slopes 55° and greater were not included in the analysis since they are less likely to accumulate the colluvium (loose, unconsolidated sediment) necessary for channelized debris flow initiation (Burns and others, 2022). The curvature raster identifies topography that is concave or convex and indicates where water and colluvium might collect or be dispersed. Debris flows tend to initiate in or near an existing drainage channel, so the distance to a channel was also included in the initiation potential (Burns and others, 2022; table 3).

The final initiation potential score is the sum of the slope, curvature, and distance values, culminating in a single value, which we then classified as high, moderate, low, or very low/no susceptibility (table 4).

Transport

Once a debris flow begins to travel down a channel, certain conditions must exist for it to continue to flow. Burns and others (2022) use channel gradient and confinement as the two primary criteria to define the transportation potential of a flowing channelized debris flow. Their tool divides the drainage network created in an earlier step (see Initiation) into 30.5-meter (100-foot) segments, which are used as the flow paths for transportation potential.

Channel gradient is the downhill slope of the channel, defined by the number of meters (feet) the channel drops per kilometer (mile) along its length. Steeper channel gradients are more likely to transport debris flows than shallower gradients, and deposition is more likely to occur where the gradient becomes shallower (Burns and others, 2022).

Channel confinement describes the degree to which lateral movement within a channel is restricted and reflects the relationship between channel width and the surrounding landscape, floodplain, or valley. The tool created by Burns and others (2022) transects the channel segments perpendicularly at 8-meter (25-foot) intervals that extend 30.5 meters (100 feet) to either side of the channel line, creating five transect lines per segment. It places points at 3-meter (9-foot) intervals along the transect lines and extracts the elevation at each point from the DTM. The tool calculates the difference between the highest and lowest elevation values for each transect line, then calculates the average of the differences for the five transect lines for each channel segment and assigns the average to that channel segment. This value defines the amount of confinement for that segment. A difference of 3 m (10 ft) along the 30.5-meter (100-foot) segment indicates low confinement (i.e. the channel can more easily shift side to side), whereas a difference of 23 m (75 ft) along the 30.5-meter (100-foot) segment indicates high confinement (i.e. the channel cannot easily shift laterally).

We used the values suggested by Burns and others (2022) for this project (table 5). The final channel transport susceptibility score is the sum of the confinement value of each segment and the channel gradient value (table 6).

Table 3. Summary of values for debris flow initiation potential

		Slope	Curvature	Distance to drainage	
Assigned Value	Category	Degrees	0.0035 m (1/100 ft)	ft	m
4	High	35 to < 55	≤ -0.4	≤ 100	≤ 30.5
3	Moderate	25 to ≤ 35	-0.4 to ≤ 0.3	100 to ≤ 200	30.5 to ≤ 61
2	Low	15 to ≤ 25	0.3 to ≤ 1.1	200 to ≤ 300	61 to ≤ 91.4
1	Very low to none	≤15	> 1.1	> 300	> 91.4

Table 4. Final debris flow initiation susceptibility scores

Score (Slope + Curvature + Distance)	Susceptibility Class
11 and 12	High
8 to 10	Moderate
5 to 7	Low
4 or less	Very low to none

Table 5. Summary of values for channel transport potential (Burns and others, 2022)

Assigned Value	Category	Confinement		Gradient
		Vertical Feet Per 100-Foot Increment	Vertical Meters Per 30.5-Meter Increment	Degrees
4	High	≥ 40	≥ 12	≥ 15
3	Moderate	20 to < 40	6 to < 12	7.5 to < 15
2	Low	10 to < 20	3 to < 6	5 to < 7.5
1	Very low to none	≤10	≤3	≤ 5

Table 6. Final channel transport susceptibility scores (Burns and others, 2022)

Score (Confinement + Gradient)	Susceptibility Class
8	High
6 and 7	Moderate
4 and 5	Low
Less than 4	Very low to none

Watershed Susceptibility to Debris Flows

A watershed is the upslope area that contributes flow to a common outlet. The tool created by Burns and others (2022) generates watersheds using standard hydrography tools in ArcGIS Pro and applies user-defined pour points (i.e. outlets) and the transport channels created in an earlier step (see Transport). Watershed susceptibility combines initiation potential and transportation potential and is based on the estimated number of initiation sites per area and the percent of transport channels with high and moderate susceptibility (Burns and others, 2022; table 7). The tool joins initiation and transport susceptibility scores to each watershed polygon and sums the values to create a final susceptibility score for that watershed (Burns and others, 2022; table 8). This score does not take into account how long it might take for debris to accumulate after an event or how much water is flowing; it assumes a sufficient volume of material that can be transported is always available and that there is always water flowing fast enough to transport it. Susceptibility zones are shown on map sheet 3.

Inundation/Deposition

Burns and others (2022) recommend modeling debris flows for three hazard scenarios: typical, intermediate, and extreme. The typical scenario is a relatively common event that has a small to medium impact and might occur every few years or decades. The extreme scenario is less common, has a much larger impact, and might occur only once per 1,000 years or less frequently Characteristics of an intermediate scenario fall between typical and extreme. Two input values are required for modeling each scenario: growth factor and maximum volume. Growth factor defines the erosion and entrainment of debris that increases the volume of a moving debris flow. The maximum volume limits how large the debris flow can grow. Input values for the typical scenario are selected and adjusted until the modeled inundation area closely matches observed debris flow extents in the area. These values are then scaled up to obtain corresponding values for the intermediate and extreme scenarios (Burns and others, 2022).

We found that growth factor was the more significant variable in determining inundation; the maximum volume rarely limited the inundation output. After iterative testing, we modeled the typical scenario with a growth factor of 0.10 m^3/m^2 (0.30 ft^3/ft^2) and a maximum volume of 100,000 m^3 (3,531,467 ft^3), and the extreme

Table 7. Summary of values for watershed potential (Burns and others, 2022)

Assigned Value	Category	Number of Estimated Potential Initiation Sites per Watershed	Percent of High and Moderate Channels in Watershed
4	High	≥ 5	≥ 50
3	Moderate	1 to < 5	25 to < 50
2	Low	0.5 to < 1	10 to < 25
1	Very low to none	< 0.5	< 10

Table 8. Final watershed susceptibility score (Burns and others, 2022)

Score (initiation site + susceptible channels)	Susceptibility Class
8	High
6 and 7	Moderate
4 and 5	Low
Less than 4	Very low to none

scenario with a growth factor of 1.0 m^3/m^2 (3.3 ft^3/ft^2) and a maximum volume of 250,000 m^3 (8,828,667 ft^3). We did not model the intermediate scenario since it falls between the other two and would not add any significant value to the map.

For both scenarios, we used the same values for concavity threshold, minimum concavity size, and minimum contributing concave area that we used in Initiation, described above. We manually selected the locations where debris flows would slow, and deposit material based on a decrease in slope gradient and where the potential for upslope initiation and transport decreased to “low” or “very low to none” (Burns and others 2022).

We used Esri’s Boundary Clean tool to smooth the final inundation raster images and then converted them to polygons to further smooth the edges and to remove unrealistic deposition spikes where the DTM appeared flat, such as across water surfaces. We also adjusted the edges of some polygons to remove areas that were likely incorrectly classified due to interpolation during production of the DTM.

Results and Discussion

Landslide Inventory and Database

The landslide inventory database includes the existing TNF landslide inventory with additional debris flow, landslide, and rockfall features identified through interpretation of lidar data and aerial imagery (map sheet 1). This project did not include field verification; therefore, many features could not be confidently assigned to a specific movement type and are classified as undifferentiated. The final database includes 294 deposits: 274 debris flows, 10 landslides, and 10 rockfalls. Of the 294 deposits, 249 are from the TNF inventory, 38 are newly mapped by this project, and 7 are from other published sources.

More than 90 percent of the landslide inventory is classified as debris flow, although some may be earthflows, mudflows, or other flow types. We identified debris flow deposits in most drainage channels, although some accumulated material may be the result of alluvial processes. Deposits may represent repeat events rather than a single failure. We also identified debris flow deposits without distinct channels. These may be complex failures that initiated as landslides and then transitioned into a debris flow as saturated material moved downslope.

The landslide category may include translational and rotational landslides, as well as possible bedrock failures associated with lineaments (e.g., small faults). We also mapped several small scarps along riverbanks that may reflect river erosion rather than landslides, and scarps on steep bedrock slopes that may be associated with rockfall.

The rockfall category may include debris fall, rockfall and rock topple. We identified rockfall along road cuts and at a few steep bedrock locations. Colluvium and talus deposits below steep bedrock slopes might also contain rockfall.

Susceptibility Maps

Shallow Landslides

In general, steeper slopes and those comprised of loose, non-cohesive soils are more susceptible to shallow landslides than gentler slopes and those with dense or cohesive soils. We used the landslide inventory as input for a frequency ratio (FR) model and found that the largest FR values are associated with steep slopes (table 1), indicating slope angle is the primary factor controlling landslide occurrence on Wrangell Island. We also found associations with slope aspect, proximity to drainages, and geology. In contrast, slope curvature, proximity to roads, and topographic wetness (TWI) did not improve model performance; however, several landslides initiated immediately downslope of a road edge and may be associated with culvert locations or other road-related features, and TWI appears to reinforce the importance of slope angle.

Eighteen inventoried landslides are located immediately downslope of roads that appear to be unpaved rural roads, and most occur within visible drainage channels. This pattern might indicate an association with culvert locations, steep embankments, or increased erosion during rain events, rather than slope failures attributed directly to road cuts.

Our FR analysis indicated that slopes greater than about 31° that are southwest- west- or northwest-facing, within 30 m (~100 ft) of a drainage, and in colluvium are the most susceptible to shallow landslide initiation. Although steep bedrock slopes account for more than 20 percent of mapped landslides on Wrangell Island, the highest susceptibility in the model is associated with steep colluvial slopes near drainages. The landslide susceptibility map highlights areas that may warrant further investigation before development (map sheet 2).

More than 90 percent of the inventoried slope failures are classified as debris flows, and 60 percent are not associated with drainages. Consequently, the FR model is dominated by debris flow initiation sites but primarily reflects susceptibility to non-channelized slope failures that transition into debris flows, rather than debris flows that are confined to existing channels.

Channelized Debris Flows

Although Burns and others (2022) incorporated the Laharz model into their channelized debris flow model, their watershed susceptibility to debris flows score and the Laharz inundation extents shown on map sheet 2 are separate outputs. Watersheds are identified as susceptible to channelized debris flows based on initiation and transport characteristics, but some might lack the volume or growth necessary for Laharz model an inundation extent.

The channelized debris flow model identified only 144 of the 274 inventoried debris flow initiation sites (i.e. 53 percent) as occurring within watersheds susceptible to initiating and transporting debris flows. According to the model, the remaining initiation sites are associated with channels and watersheds that are too small, have slopes that are too flat, are insufficiently concave, or exhibit a combination of these characteristics to initiate and/or transport a channelized debris flow. One likely explanation is that many of the inventoried failures may have initiated as translational or rotational landslides and transitioned into debris flows due to soil saturation and ongoing rainfall, with or without an established channel. This represents a more complex failure process than can be simulated using the channelized debris flow model. Another contributing factor may be that small groundwater seeps, low relief drainage features, and unchanneled sheet flow are not captured in the lidar-derived terrain model and therefore cannot be modeled with a lidar-based method. Despite these limitations, the inundation areas shown on map sheet 3 identify the larger drainage systems that are most susceptible to channelized debris flows and the areas where debris is most likely to deposit.

Because map sheet 2 primarily reflects non-channelized slope failures, and map sheet 3 evaluated channelized debris flow routing, the two maps should be used together to provide a more complete understanding of landslide hazards on Wrangell Island.

Areas of Concern

Near the City of Wrangell, the modeled susceptibility to shallow landslides is generally low to no susceptibility, except on the southwest-facing slopes of Mt. Dewey and the hill immediately east of town, where the steep slopes are moderately to highly susceptible. The municipal water reservoirs just outside the city are critical infrastructure and our analysis indicates they are in an area of high shallow landslide susceptibility and possible inundation by debris flows. Slope failures here could temporarily reduce water quality through increased sediment, or by displacing water within the reservoirs. Similarly, the area between approximately mileposts 4 to 5 of Pat Creek Road has a high susceptibility to both shallow landslides and debris flow inundation. In addition, bedrock road cuts along Zimovia Highway are known rockfall locations that require ongoing monitoring and maintenance. This study did not evaluate other slope failure mechanisms such as liquefaction or lateral spreading triggered by seismic shaking.

Intended Use and Limitations

The intended use of this report and associated maps is to help identify areas that may be susceptible to slope failure, to provide a basis for regional planning and increased resiliency, and to help identify areas where more detailed landslide mapping is warranted. Limitations of the input data and modeling methods are such that the maps are not suitable to answer site-specific or legal questions. The maps should only be used for regional- or community-scale purposes and should not be viewed at scales other than the published map scale of 1:25,000. They are not suitable for land-use regulation, building-code development, or to answer legal questions.

Mapping limitations

- This project was desktop-based, did not include field verification, and relied on available datasets.
- Lidar provides a snapshot view of the landscape at the time of data collection; therefore, maps based on lidar data interpretation may become less accurate as new landslides occur or improved technology becomes available.
- Lidar data interpretation may also change as new mapping techniques are developed.
- While every reasonable effort was made to identify all slope failures, limitations in lidar data, available imagery, vegetation cover, and the lack of field verification meant that some slope failures were likely missed, overlooked, or misinterpreted.

Shallow landslide susceptibility model limitations

- The FR analysis used post-landslide lidar data; therefore, mapped landslide initiation sites may not represent pre-failure slope conditions.
- FR is a statistical method that identifies associations rather than causation, and the resulting susceptibility values represent relative likelihood rather than absolute probability.
- FR assumes the selected conditioning factors are independent of each other and does not capture more complex interactions between factors.

Channelized debris flow model limitations

- Debris flow modeling is based on estimated growth factors and volumes. Actual debris flow behavior may differ from the modeled results.
- Buildings, bridges, culverts, changes in topography, and mitigation measures can alter debris flow paths.
- The modeling does not account for differences in material composition. For example, woody debris entrained within the debris flow slurry can affect flow behavior and runout length and width.
- Lidar-based analysis cannot always distinguish between natural elevation changes (e.g. landslide scour and deposition) and man-made structures (e.g. buildings and other structures).

Intended use

- DGGS is not a regulatory agency; therefore, this report and maps are non-regulatory.

Conclusion

DGGS completed this landslide hazard assessment for the City and Borough of Wrangell by developing a landslide inventory and database, a map of modeled shallow landslide susceptibility, and a map of modeled channelized debris-flow initiation and runout. Together these products provide a regional assessment of slope failure hazards that can support community planning, emergency preparedness, and the identification of areas where more detailed investigations may be warranted. The maps identify areas that are relatively more susceptible to slope failure but do not predict the timing, probability, or reoccurrence intervals of future landslides. Site-specific geologic and geotechnical investigations should be completed prior to development in potentially hazard-prone areas. The results presented herein are for informational purposes only and are not suitable for legal, engineering, or surveying uses.

Acknowledgments

This work was funded by the Federal Emergency Management Agency (FEMA) Cooperative Technical Partnership (CTP) Program grant number EMS-2024-CA-05006. We thank Katreen Wikstrom Jones and our other reviewers for their expertise and thoughtful comments that helped improve the quality of this product.

References

Alaska Department of Transportation & Public Facilities, 2022, Geo. Event Tracker-download event data. https://akdot.maps.arcgis.com/sharing/rest/content/items/44a003d1b33945b0ba5284ca9abddd14/data

Beven, K.J., Kirkby, M.J., 1979, A physically based, variable contributing area model of basin hydrology: Hydrological Sciences Bulletin 24(1), 43-69. https://doi.org/10.1080/02626667909491834

Bobbitt, Zach, 2021, How to create a ROC curve in Excell (step-by-step): Statology, accessed October 2025. https://www.statology.org/roc-curve-excel/

Brew, D.A., 1997a, Reconnaissance geologic map of the Petersburg B-1 Quadrangle, southeastern Alaska: U.S. Geological Survey Open-File Report 97-156-C, 20 p., 1 sheet, scale 1:63,360. https://dggs.alaska.gov/pubs/id/12814

Brew, D.A., 1997b, Reconnaissance geologic map of the Petersburg B-2 Quadrangle, southeastern Alaska: U.S. Geological Survey Open-File Report 97-156-D, 21 p., 1 sheet, scale 1:63,360. https://dggs.alaska.gov/pubs/id/12815

Burns, W.J., Franczyk, J.J., and Calhoun, N.C., 2022, Protocol for channelized debris flow susceptibility mapping: Oregon Department of Geology and Mineral Industries Special Paper 53, 89 p. https://pubs.oregon.gov/dogami/sp/SP-53/p-SP-53.htm

Burns W.J., and Madin I.P., 2009, Protocol for inventory mapping of landslide deposits from light detection and ranging (lidar) imagery: Oregon Department of Geology and Mineral Industries Special Paper 42, 30 p. https://www.oregongeology.org/pubs/sp/p-SP-42.htm

Burns W.J., Madin I.P., and Mickelson, K.A., 2012, Protocol for shallow landslide susceptibility mapping: Oregon Department of Geology and Mineral Industries Special Paper 45, 32 p. https://www.oregongeology.org/pubs/sp/p-SP-45.htm

Division of Homeland Security and Emergency Management, 2023, State of Alaska state hazard mitigation plan, p. 465. ready.alaska.gov/Mitigation/SHMP

Esri, n.d., ArcGIS Pro 3.3 Help Curvature function, accessed December 2, 2025, https://pro.arcgis.com/en/pro-app/3.3/help/analysis/raster-functions/curvature-function.htm

Es-smairi, Abderrazzak, Elmoutchou, Brahim, Mir, R.A., Ouazani-Touhami, Abdelouahed, Namous, Mustapha, 2023, Delineation of landslide susceptible zones using Frequency Ratio (FR) and Shannon Entropy (SE) models in northern Rif, Morocco: Geosystems and Geoenvironment, 2(4), 100195. https://doi.org/10.1016/j.geogeo.2023.100195

Fawcett, Tom, 2006, An introduction to ROC analysis: Pattern Recognition Letters, 27(8), p. 861-874. https://doi.org/10.1016/j.patrec.2005.10.010

Highland, L.M., and Bobrowsky, Peter, 2008, The landslide handbook—A guide to understanding landslides: Reston, Virginia, U.S. Geological Survey Circular 1325, 129 p. https://pubs.usgs.gov/circ/1325/

Hubbard, T.D., Daanen, R.P., and Stevens, D.S.P., 2025, Debris flow hazard evaluations for multi-hazard risk mapping in Sitka, Alaska: Alaska Division of Geological & Geophysical Surveys Report of Investigation 2024-2, 14 p., 6 sheets, scale 1:20,000. https://doi.org/10.14509/30187

Karl, S.M., Haeussler, P.J., and McCafferty, Anne, 1999, Reconnaissance geologic map of the Duncan Canal-Zarembo Island area, southeastern Alaska: U.S. Geological Survey Open-File Report 99-168, 30 p., 1 sheet. https://pubs.usgs.gov/of/1999/of99-168/

Lee, Saro, Talib, J.A., 2005, Probabilistic landslide susceptibility and factor effect analysis: Environmental Geology, 47, 482-990 p. https://www.researchgate.net/publication/226285379_Probabilistic_landslide_susceptibility_and_factor_effect_analysis

Lemke, R.W., 1974, Reconnaissance engineering geology of the Wrangell area, Alaska, with emphasis on evaluation of earthquake and other geologic hazards: U.S. Geological Survey Open-File Report 74-1062, 103 p., 1 sheet, scale 1:7,200. https://dggs.alaska.gov/pubs/id/11017

Nicolazzo, J.A., and Larsen, M.C., 2025a, Alaska landslide inventory database: Alaska Division of Geological & Geophysical Surveys Digital Data Series 23, 14 p. https://doi.org/10.14509/31697

Nicolazzo, J.A., and Larsen, M.C., 2025b, Landslide hazard susceptibility mapping in Haines, Alaska: Alaska Division of Geological & Geophysical Surveys Report of Investigation 2024-8, 16 p., 3 sheets, scale 1:25,000. https://doi.org/10.14509/31309

Nicolazzo, J.A., Wikstrom Jones, K.M., Salisbury, J.B., and Horen, K.C., 2024, Post-landslide elevation changes detected from multi-temporal lidar surveys of the November 2023 Wrangell, Alaska, landslides: Alaska Division of Geological & Geophysical Surveys Preliminary Interpretive Report 2024-2, 22 p. https://doi.org/10.14509/31124

Salisbury, J.B., 2024, Landslide hazard susceptibility mapping in Homer, Alaska: Alaska Division of Geological & Geophysical Surveys Report of Investigation 2024-3, 21 p., 3 sheets, scale 1:13,500. https://doi.org/10.14509/31155

Schilling, S.P., 1998, LAHARZ; GIS programs for automated mapping of lahar-inundation hazard zones: U.S. Geological Survey Open-File Report 98-638, 80 p. doi.org/10.3133/ofr98638

Slaughter, S. L.; Burns, W. J.; Mickelson, K. A.; Jacobacci, K. E.; Biel, Alyssa; Contreras, T. A., 2017, Protocol for landslide inventory mapping from lidar data in Washington State: Washington Geological Survey Bulletin 82, 27 p. text, with 2 accompanying ESRI file geodatabases and 1 Microsoft Excel file. http://www.dnr.wa.gov/Publications/ger_b82_landslide_inventory_mapping_protocol.zip

Strauch, Ronda, Istanbulluoglu, Erkan, Riedel, Jon, 2019, A new approach to mapping landslide hazards: a probabilistic integration of empirical and physically based models in the North Cascades of Washington, USA, Natural Hazards Earth System Sciences, 19, 2477–2495. https://doi.org/10.5194/nhess-19-2477-2019

U.S. Department of Agriculture, 2017, U.S. General Soil Map (STATSGO2) by State, [accessed January 6, 2025] https://nrcs.app.box.com/v/soils/folder/18247487156

U.S. Fish and Wildlife Service, 2025, Wetlands data by state, [accessed January 6, 2025] https://www.fws.gov/program/national-wetlands-inventory/download-state-wetlands-data

U.S. Forest Service, 2024a, Tongass National Forest: Tongass Landslide Areas: U.S. Department of Agriculture Forest Service. [accessed April 2024] https://data.fs.usda.gov/geodata/edw/datasets.php?xmlKeyword=tongass

U.S. Forest Service, 2024b, Tongass National Forest: Tongass Landslide Initiation: U.S. Department of Agriculture Forest Service. [accessed April 2024] https://data.fs.usda.gov/geodata/edw/datasets.php?xmlKeyword=tongass

Zechmann, J.M., Wikstrom Jones, K.M., and Wolken, G.J., 2023, Lidar-derived elevation data for Wrangell Island, Southeast Alaska, collected July 2023: Alaska Division of Geological & Geophysical Surveys Raw Data File 2023-28 v. 1.1, 14 p. https://doi.org/10.14509/31098

Zechmann, J.M., Wikstrom Jones, K.M., and Wolken, G.J., 2024, Lidar-derived elevation data for Wrangell Island, Southeast Alaska, collected November 28-29, 2023: Alaska Division of Geological & Geophysical Surveys Raw Data File 2024-1, 9 p. https://doi.org/10.14509/31106